

Monomial Gamma Monte Carlo Sampling

Yizhe Zhang^{*1}, Xiangyu Wang^{†2}, Changyou Chen^{‡1}, Kai Fan^{§2} and Lawrence Carin^{¶1}

¹Department of Electrical and Computer Engineering, Duke University

²Department of Statistical Science, Duke University

Abstract

We unify slice sampling and Hamiltonian Monte Carlo (HMC) sampling by demonstrating their connection under the canonical transformation from Hamiltonian mechanics. This insight enables us to extend HMC and slice sampling to a broader family of samplers, called monomial Gamma samplers (MGS). We analyze theoretically the mixing performance of such samplers by proving that the MGS draws samples from a target distribution with zero-autocorrelation, in the limit of a single parameter. This property potentially allows us to generating decorrelated samples, which is not achievable by existing MCMC algorithms. We further show that this performance gain is obtained at a cost of increasing the complexity of numerical integrators. Our theoretical results are validated with synthetic data and real-world applications.

1 Introduction

Markov Chain Monte Carlo (MCMC) (Robert & Casella, 2004) stands as a fundamental approach for probabilistic inference in many computational statistics problems. A pivot question in MCMC is to design methods to efficiently draw samples from an unnormalized density function. Two auxiliary-variable sampling schemes, Hamiltonian Monte Carlo (HMC) (Neal, 2011; Duane et al., 1987) and the slice sampler (Neal, 2003), have been introduced for tackling this challenge. HMC exploits gradient information to propose distant samples along the trajectory of a contour of the Hamiltonian, introducing momentum as an auxiliary variable. Compared to the random proposal in Metropolis-Hastings (Neal, 2003) or Gibbs sampling, HMC is able to propose large moves with acceptance ratio close to one (Neal, 2011). Recent attempts toward improving HMC have been done by leveraging geometric manifold information (Girolami & Calderhead, 2011), using better numerical integrators (Chao et al., 2015), and considering special likelihood forms (Murray et al., 2009). The limitations of HMC, however, include being sensitive to parameter tuning and being restricted to continuous distributions. These issues

are partially solved by using adaptive leap-frog steps (Homan & Gelman, 2014), and transforming the problem of sampling discrete distributions into continuous distributions (Pakman & Paninski, 2013; Zhang et al., 2012).

The slice sampler, as another auxiliary-variable-based MCMC method, has recently received extensive attention. The sampling procedure of slice sampler alternates between drawing samples from the target distribution and drawing the uniformly distributed slice variables. One problem of the slice sampler is the intractability of solving for the slice interval. As a result, adaptive methods are often applied (Neal, 2003). It has been shown that in some cases, slice sampling is more efficient than Gibbs sampling and Metropolis-Hastings schemes, due to the adaptability of the sampler to the scale of the region currently being sampled (Neal, 2003).

Despite the success of slice sampling and HMC, little research has been done to investigate their connections, as well as their sampling efficiency. In this paper, using the canonical transformation from classical mechanics, we show that performing a generalized HMC can be seen as performing generalized slice sampling. Based on this relationship, we develop theory to analyze this broad family of auxiliary-variable-based samplers. We prove that the one-time-lag autocorrelation converges asymptotically to zero, leading to potentially decorrelated samples. We further show that such samplers can be conducted in an HMC fashion using numerical integrators, which can be seen as a drop-in replacement for standard HMC leap-frog steps. Finally, we point out that these theoretical gains come at a cost of increasing numerical difficulty. We validate our theory on both synthetic data and real-world problems, including Bayesian Logistic Regression (BLR) and Independent Component Analysis (ICA), for which we compare the mixing performance of our approach with standard HMC.

2 Canonical transformation for Hamiltonian dynamics

To make the connection between HMC (reviewed in the Appendix) and slice sampling, we review and extend the

theory of *canonical transformation* and the *Hamilton-Jacobi equation* (HJE) from classic mechanics (Goldstein, 1965). In the following theoretical development, we focus on the univariate case for simplicity. Results of the multivariate case follow similarly.

Specifically, in our framework, instead of using a Gaussian kinetic function, we propose a general form of kinetic energy, defined as* $K(p) = |p|^{1/a}$, such that the Hamiltonian is $H(x, p) = E(x) + |p|^{1/a}$. In the *canonical transformation*, the original HMC system (H, x, p, t) is transformed to a new space denoted (H', x', p', t) , and the transformation $(H, x, p, t) \rightarrow (H', x', p', t)$ satisfies the *Hamilton's principle* (Goldstein, 1965) described by:

$$\lambda(p \cdot \dot{x} - H) = p' \cdot \dot{x}' - H' + \frac{dG}{dt}, \quad (1)$$

where $\lambda \in \mathbb{R}$ is a constant, G is a generating function[†], which uniquely characterizes a canonical transformation, and can be of several types (Taylor, 2005). Here we adopt a type-2 generating function defined as $G \triangleq -x' \cdot p' + S(x, p', t)$, with $S(x, p', t)$ being the *Hamilton's principal function*, with explicit form defined below.

From (1), due to the independency of x and p' , the following equations must hold:

$$p = \frac{\partial S}{\partial x}, \quad x' = \frac{\partial S}{\partial p'}, \quad H'(x', p') = H(x, p) + \frac{\partial S}{\partial t}. \quad (2)$$

The Hamilton-Jacobi equation sets the new Hamiltonian H' to be zero, *i.e.*,

$$H(x, p) + \frac{\partial S}{\partial t} = H'(x', p') = 0. \quad (3)$$

An important property of the Hamilton-Jacobi equation is that under this transformation the motion of particles collapses into a point in the new space, *i.e.*, (x', p') are constant over time.

We now specify $S(x, p', t) = W(x) - p't$, where $W(x)$ is an unknown function of x . From (3) and (2), we can obtain

$$H(x, p) + \frac{\partial S}{\partial t} = E(x) + \left| \frac{dW(x)}{dx} \right|^{\frac{1}{a}} - p' = 0. \quad (4)$$

This implies that $p' = H$, *i.e.*, the *generalized momentum* in the new phase space (x', p') , represents the total Hamiltonian in the original space. Define $\mathbb{X} \triangleq \{x : H - E(x) \geq 0\}$ as the *slice interval*. Solving (4) gives

$$W(x) = \int_{x_{min}}^{x(t)} f(z)^a dz + C, \\ f(z) = \begin{cases} H - E(z), & z \in \mathbb{X} \\ 0, & z \notin \mathbb{X} \end{cases},$$

*It can be shown that the HJE can be applied as long as $K(p)$ is symmetric *w.r.t.* $p = 0$ and monotonically increasing when $p \geq 0$.

[†] G is a function of one old canonical coordinate (x or p), into one new canonical coordinate (x' or p'), and (possibly) time, t .

where $x_{min} = \min\{x : x \in \mathbb{X}\}$. Applying Fubini's theorem to (2) gives

$$x' = \frac{\partial S}{\partial p'} = \frac{\partial W}{\partial H} - t = \frac{1}{a} \int_{x_{min}}^{x(t)} f(z)^{a-1} dz - t. \quad (5)$$

Note that because x' is a constant in the new space, *e.g.*, $x' = \alpha$, from (5), the time, t , can be shown to be in the following range (considering a single period of the movement):

$$t \in \left[-\alpha, -\alpha + \frac{1}{a} \int_{\mathbb{X}} [H - E(z)]^{a-1} dz \right]. \quad (6)$$

As a result, to sample the Hamiltonian in the new space, we only need to sample t uniformly from the domain in (6). Note that the integral in (5) can be interpreted (up to normalization) as a Cumulative Density Function (CDF) of x . As in inverse transform sampling, uniformly sampling t from (6) and solving x from (5), is equivalent to directly sampling from following density

$$p(x) \propto [H - E(x)]^{a-1}, \quad s.t., x \in \mathbb{X}. \quad (7)$$

This procedure reveals the connections between the slice sampler and the HMC, which is elaborated on in the next section. Note that when the kinetics takes the form $K(p) = |p|^{1/a}/m$, the above holds as for $K(p) = |p|^{1/a}$.

3 Monomial Gamma distribution

The special family of kinetic functions $K(p) = \frac{|p|^{1/a}}{m}$ with $a > 0$ and $m > 0$, as we defined above, leads to a distribution where p is drawn from

$$\pi(p; m, a) = \frac{m^{-a}}{2\Gamma(a+1)} e^{-\frac{|p|^{1/a}}{m}}. \quad (8)$$

We denote this as the *monomial Gamma* (MG) distribution, where m is the *mass parameter*, and a is the *monomial parameter*. Note that this is the exponential power distribution with zero-mean (Nadarajah, 2005). This distribution has been leveraged as the shrinkage prior for the regression coefficients in the Bayesian bridge estimator (Fu, 1998), and has deep connections with the p -norm in vector spaces. When $a = 1/2$, this distribution degenerates to the Gaussian distribution, and the kinetic function becomes that of standard HMC. When $a = 1$, it leads to the double-exponential (Laplace) distribution, $p \sim \mathcal{L}(0, m)$.

We summarize some useful properties of the MG distribution in the Appendix, here we focus on generating random variables from it. To this end, one can first draw $G \sim \text{Gamma}(a, m)$ and a uniform sign variable $S \sim \{-1, 1\}$, then $S \cdot G^a$ follows the monomial Gamma distribution. We call the resulting HMC sampler based on this potentially non-Gaussian kinetic function $K(p)$, the *Monomial*

Gamma Hamiltonian Monte Carlo (MG-HMC). For simplicity, we define the multivariate Monomial Gamma distribution as a product of independent univariate Monomial Gamma distributions.

4 Formulating HMC as a slice sampler in the canonical space

Based on (7) and the Monomial Gamma kinetics $K(p) = |p|^{1/a}/m$, it is possible to design a sampler to perform MG-HMC in the canonical space, as shown in Algorithm 1.

Algorithm 1 MG-HMC in canonical space

Input: Total sample size T , potential energy $E(x)$, kinetics $K(p; m, a)$.

Output: Sample results, $\{x_0, \dots, x_T\}$.

Initialization: Choose initial sample point x_0 .

for $t = 1$ to T **do**

 Sample $p_t \sim \text{MonomialGamma}(m, a)$.

 Compute Hamiltonian: $H_t = E(x_t) + K(p_t)$.

 Find $\mathbb{X} \triangleq \{x : x \in \mathbb{R}; E(x) \leq H_t\}$.

 Sample $x_{t+1} | H_t \propto [H_t - E(x_{t+1})]^{a-1}; x \in \mathbb{X}$.

end for

To see clearly how Algorithm 1 relates to the slice sampler, we denote $y_t = e^{-H_t}$, and instead of directly sampling (p, x) as in Algorithm 1, we sample (y, x) . The conditional updates for the above sampling procedure can be rewritten as below, yielding a *Monomial Gamma Slice sampler* (MG-SS, Algorithm 2) with conditional distributions

$$p(y_t | x_t) = \frac{1}{\Gamma(a)f(x_t)} [\log f(x_t) - \log y_t]^{a-1}, \quad (9)$$

$$s.t. 0 < y_t < f(x_t)$$

$$q(x_{t+1} | y_t) = \frac{1}{Z_2(y_t)} [\log f(x_{t+1}) - \log y_t]^{a-1}, \quad (10)$$

$$s.t. f(x_t) > y_t$$

where $f(x) = e^{-E(x)}$ is an unnormalized density, and $Z_1 \triangleq \int f(x) dx$ and $Z_2(y) \triangleq \int_{f(x) > y} [\log f(x) - \log y]^{a-1} dx$ are the normalization constants (partition functions). Note that when $a \rightarrow \infty$, the conditional distribution $q(x|y) \rightarrow \delta(x_m)$, where $\delta(x_m)$ is the *Dirac delta function* centered at the mode (assuming the target distribution is unimodal) of $p(x)$.

Interestingly, when $a = 1$, Algorithm 2 recovers exactly the update steps in standard slice sampling, where the conditional distributions are uniform. For other cases, we iteratively draw from non-uniform distributions for both auxiliary variable y and target variable x . Using the same argument from the convergence analysis of standard slice sampling (Neal, 2003), this iterative sampling procedure

Algorithm 2 Monomial Gamma Slice sampler

Input: Total sample size T , MG parameter a .

Output: Sample results, $\{x_0, \dots, x_T\}$.

Initialization: Choose initial sample point x_0 .

for $t = 1$ to T **do**

 Sample y_t from Equation (9).

 Sample x_t from Equation (10).

end for

will converge to an invariant joint distribution

$$p(x, y) = \begin{cases} \frac{1}{\Gamma(a)Z_1} [\log f(x) - \log y]^{a-1} & \text{if } 0 < y < f(x) \\ 0, & \text{otherwise} \end{cases}$$

The marginal distribution for x recovers the target distribution as $f(x)/Z_1$, while the marginal distribution of y is given by

$$p(y) = Z_2(y)/[\Gamma(a)Z_1]. \quad (11)$$

The MG-SS for $0 < a < 1$, $a = 1$ and $a > 1$ are illustrated in Figure. 1. When $0 < a < 1$, the conditional distribution $p(y_t | x_t)$ is skewed towards the current unnormalized density value $f(x_t)$. The conditional draw of $q(x_{t+1} | y_t)$ encourages taking samples with smaller density value, within the domain of the slice interval \mathbb{X} (as defined in Algorithm 1). On the other hand, when $a > 1$ the sampler has an opposite behavior, where draws of y_t tend to take smaller values, while draws of x_{t+1} encourage sampling from those with large density function values.

Intuitively, setting a to be small makes the auxiliary variable, y_t , stay close to $f(x_t)$, thus x_{t+1} is close to x_t . As a result, a larger a seems more desirable. We will theoretically verify this intuition in the following sections.

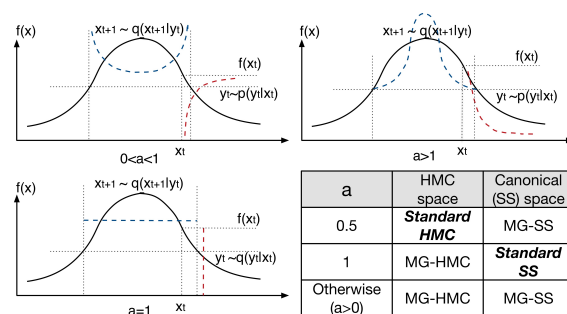


Figure 1: MG-HMC and equivalent MG slice sampler. Red and blue dashed lines denote the conditionals $p(y_t | x_t)$ and $q(x_{t+1} | y_t)$, respectively.

5 MG sampling with Hamiltonian dynamics

The connection revealed by Section 4 allows us to tackle the same sampling task by either MG-SS or MG-HMC. Unfortunately, performing analytic MG-SS (analytically perform Algorithm 2) requires: 1) analytically solving for the slice interval \mathbb{X} , which is typically infeasible for multivariate cases (Neal, 2003); or 2) analytically computing the integral $Z_2(y)$ over \mathbb{X} , implied by the non-uniform conditionals from MG-SS. We note that it is possible to adaptively estimate \mathbb{X} using schemes like “doubling” and “shrinking” strategies (Neal, 2003), and numerically compute the normalization constant, $Z_2(y)$.

On the other hand, performing MG-HMC using a numerical integrator is much more convenient. Therefore, we resort to MG-HMC instead of MG-SS, where the Hamiltonian dynamics step of MG-HMC corresponds to the slicing step of MG-SS in (10). Specifically, consider multivariate case: for each iteration, the momentum \mathbf{p} is initialized by sampling from $\text{MG}(m\mathbf{I}, a)$, where each $\mathbf{p}^{(d)}$ is drawn as in Algorithm 1. Then, we use the second order Störmer-Verlet integration (Neal, 2011) to perform the Hamiltonian dynamics updates. The leap-frog procedures are given by

$$\mathbf{p}_{t+1/2} = \mathbf{p}_t - \frac{\epsilon}{2} \nabla E(\mathbf{x}_t) \quad (12)$$

$$\mathbf{x}_{t+1} = \mathbf{x}_t + \epsilon \nabla K(\mathbf{p}_{t+1/2}) \quad (13)$$

$$\mathbf{p}_{t+1} = \mathbf{p}_{t+1/2} - \frac{\epsilon}{2} \nabla E(\mathbf{x}_{t+1}), \quad (14)$$

where $\nabla K(\mathbf{p}) = \text{sign}(\mathbf{p}) \cdot \frac{1}{ma} |\mathbf{p}|^{1/a-1}$. Two practical issues arise in the numerical integration. First, when $a = 1$, $[\nabla K(\mathbf{p})]_d = 1/m$ for any dimension d , independent of \mathbf{x} and \mathbf{p} . To avoid moving on a grid, we employ a random step size ϵ from a uniform distribution within a non-negative range $[r_1, r_2]$. Second, when $a > 1/2$, the contour in the phase space, (\mathbf{x}, \mathbf{p}) , has at least 2^D (D denotes the total dimension) non-differentiable points (turnovers), at each intersection point with the hyperplane $\mathbf{p}^{(d)} = 0, d \in \{1 \cdots D\}$. Directly applying the Störmer-Verlet integration would lead to high integration errors when the dimensionality becomes large. To remedy this issue, we use an analog to the “reflection” action (Neal, 2011). The intuition comes from the fact that the contour is symmetric with hyperplanes $\mathbf{p}^{(d)} = 0$ for each dimension d . In (12) and (14), whenever the d -th dimension(s) of the momentum change sign, we recoil the point of these dimension(s) to the previous iteration, and negate the momentum of these dimension(s), (i.e., $\mathbf{x}_{t+1}^{(d)} = \mathbf{x}_t^{(d)}, \mathbf{p}_{t+1}^{(d)} = -\mathbf{p}_t^{(d)}$). This strategy performs well in low-dimensional phase space, but may suffer from sticky behavior in high-dimensional cases. This is because the probability of a sign change occurrence is high; recall there are at least 2^D turnovers. Discussions on possible remedies for this problem are discussed in the following sections.

6 Theoretical analysis

This section analyzes some key theoretical properties of the proposed MG sampler, with proofs given in the Appendix.

6.1 Convergence properties

Following Tierney & Mira (1999) and Robert & Casella (2004), we show in the Appendix that the MG-SS is reversible and *Harris ergodic*. As a result, the chain is guaranteed to uniquely and asymptotically converge to the target distribution. This also implies that for certain $g : \mathcal{X} \rightarrow \mathbb{R}$, the sample-based estimator \bar{g} almost surely converges to the expectation with respect to the true distribution (Robert & Casella, 2004). Next, following standard slice sampler (Tierney & Mira, 1999), we show that MG-SS is uniformly ergodic under the *Doebelin’s conditions* (Isaac, 1963) in Proposition 1[‡].

Proposition 1 (Uniform ergodicity) *Suppose $f(\cdot)$ is bounded and has bounded support. If $a \geq 1$, the analytic MG-SS is uniformly ergodic.*

Geometric ergodicity is a less restrictive property compared to the uniform ergodicity. However, establishing such ergodicity for general cases requires demonstrating the *drift* and *minorization* conditions (Johnson, 2009). Roberts & Rosenthal (1998) has showed that for any univariate log-concave density $f(\cdot)$, the resulting Markov chain associated with the slice sampler is geometrically ergodic, and the quantitative convergence bounds are available. In fact, a necessary condition for any multivariate density being geometrically ergodic is that $y\mu'(y)$ is non-increasing with respect to y , where $\mu(y)$ is the Lebesgue measure of the slice interval $\{w : f(w) \geq y\}$, and the prime symbol denotes derivative *w.r.t.* y . In MG-SS, we hypothesize this requires $yZ_2'(y)$ to be non-increasing, however we leave the formal verification for future work.

6.2 One-time-lag autocorrelation

For clarity, we focus on sampling from a univariate distribution $p(x) \propto e^{-E(x)}$. We first investigate the impact of the monomial parameter a on the one-time-lag *autocorrelation function* (ACF), $\rho(1)$, as a first step to understand the limiting behavior of the mixing performance when $a \rightarrow \infty$. The $\rho(1)$ is defined as

$$\rho(1) = \text{corr}(x_t, x_{t+1}) = \frac{\mathbb{E}x_t x_{t+1} - (\mathbb{E}x)^2}{\text{Var}(x)}, \quad (15)$$

[‡]We hypothesize that this proposition holds for $0 < a < 1$, however we leave it for further investigation.

From (9) and (10), noticing that the conditional density $p(x_t|y_t)$ and $p(x_{t+1}|y_t)$ have the same form, we have

$$\begin{aligned}\mathbb{E}x_t x_{t+1} &= \mathbb{E}_{p(y_t)}[\mathbb{E}_{p(x_t|y_t)}x_t \mathbb{E}_{p(x_{t+1}|y_t)}x_{t+1}] \\ &= \mathbb{E}_{p(y_t)}[\mathbb{E}_{q(x_{t+1}|y_t)}x_{t+1}]^2,\end{aligned}\quad (16)$$

where $q(x|y)$ is the conditional distribution defined in (10). From (16) and (15), when $p(x)$ is symmetric at $x = 0$, $\mathbb{E}_{q(x_{t+1}|y_t)}x_t = (\mathbb{E}x)^2$, which gives $\rho(1) = 0$.

Consider equation (16). The Jensen's inequality and stationarity implies

$$\mathbb{E}x_t x_{t+1} \leq \mathbb{E}_{p(y)}[\mathbb{E}_{q(x|y)}x^2] = \mathbb{E}x^2 \triangleq \mathcal{U},$$

which trivially gives $\rho(1) \leq 1$. The last equality follows because the marginal of the joint density $p(x, y)$ is the target distribution. The lower bound of $\mathbb{E}x_t x_{t+1}$ can be obtained as

$$\mathbb{E}x_t x_{t+1} \geq [\mathbb{E}_{p(y)}\mathbb{E}_{q(x|y)}x]^2 = (\mathbb{E}x)^2 \triangleq \mathcal{L}.\quad (17)$$

This indicates that $\rho(1) \geq 0$. Note that the equality holds when $\mathbb{E}_{q(x|y)}x$ is independent of y . To formally describe the limiting behaviour of $\rho(1)$. We then establish the following proposition.

Proposition 2 (Distillation) *Suppose $p(x) \propto g(x)^a$ is a well-defined probability density for $x \in \mathcal{D}$, where $\mathcal{D} \subseteq \mathcal{R}^d$, $g(x)$ is a non-negative integrable function, and is thrice differentiable with the third-order derivative being bounded. Define $\mathcal{M} = \{x : x = \operatorname{argmax}_x g(x)\}$ to be the finite collection of all maximum point(s) of $g(x)$. Assuming $g(x)$ is locally concave on \mathcal{M} , one can obtain,*

$$\lim_{a \rightarrow \infty} \mathbb{E}_{p(x)}x = \lim_{a \rightarrow \infty} \frac{\int x g(x)^a dx}{\int g(x)^a dx} = \mathbb{E}_{u(x)}x \cdot 1(x \in \mathcal{M}),$$

where $u(x) \propto -\nabla^2 g(x)$ is a probability measure on \mathcal{M} .

Intuitively, Proposition 2 states that when $a \rightarrow \infty$, the limiting expectation of distribution $p(x; a)$ will be distilled to the expectation over the domain that maximizes $g(x)$. Assume that our target density function contains no singular points, and $E(x) = -\log f(x)$ has minimum value. From Proposition 2, for any feasible H , when $a \rightarrow \infty$, we can obtain $\mathbb{E}_{q(x|H)}x = \mathbb{E}_{u(x)}x$, $x \in \mathcal{M}$, which are the expectation of the maximum point(s) of $g(x) \triangleq H - E(x)$ (or, minimum point(s) of $E(x)$) that do not depend on H . Based on this result, one can establish a Theorem 3 (proved in the Appendix) describing the limiting behavior of $\rho(1)$,

Theorem 3 *For analytic MG-SS parameterized by a , the one time lag autocorrelation $\rho(1)$ asymptotically approaches zero when $a \rightarrow \infty$.*

6.3 Effective sample size

It is known that the variance of a Monte Carlo estimator is determined by its Effective Sample Size (ESS) (Brooks et al., 2011), defined as $\text{ESS} = N/(1 + 2 \times \sum_{h=1}^{\infty} \rho(h))$. The h -time-lag autocorrelation function $\rho(h)$ can be formulated as

$$\rho(h) = \frac{\mathbb{E}_{p(x)}[\mathbb{E}_{\kappa_h(x_{t+h}|x)}x_{t+h}x] - (\mathbb{E}x)^2}{\text{Var}(x)},\quad (18)$$

where, $\kappa_h(x_{t+h}|x_t)$ represents the h -order transition kernel, which can be calculated in a recursive manner as:

$$\begin{aligned}\kappa_1(x_{t+1}|x_t) &= \int q(x_{t+1}|y_t)p(y_t|x_t)dy_t, \\ \kappa_h(x_{t+h}|x_t) &= \int \kappa_{h-1}(x_{t+1}|x_t)\kappa_1(x_{t+h}|x_{t+1})dx_{t+1}.\end{aligned}$$

We state the following property for the $\rho(h)$ in the MG sampler.

Proposition 4 *The h -order autocorrelation for analytic MG-SS, $\rho(h)$, is non-negative.*

If the MG sampler is uniformly ergodic, one can obtain that the total variance distance between the h -th transition kernel and $p(x)$ is bounded by $M(x)t^h$, where $M(x)$ is a bounded function and $0 < t < 1$ (Rosenthal, 1995). Under the condition that $\text{Var}_{\kappa_h(x_0|x)}x$ is bounded and the uniform ergodicity holds, one can demonstrate that $\rho(h)$ is bounded by $Ct^{h/2}$, where C is a positive constant. If we further assume that $\rho(h)$ is monotonically decreasing, one can show that, $\lim_{a \rightarrow \infty} \text{ESS} = N$. Details and further discussion are provided in the Appendix.

6.4 Case study

We consider a toy example with analytically available $\rho(h)$ and ESS to verify our theory. We consider the exponential distribution, $\text{Exp}(\theta)$, with energy function given by $E(x) = \theta x$, $x \geq 0$. After some algebra (see details in the Appendix), we get

$$\rho(1) = \frac{1}{a+1}, \quad \rho(h) = \frac{1}{(a+1)^h}, \quad \text{ESS} = \frac{Na}{a+2}.$$

These results agree with Theorem 3, Proposition 4 and related arguments. Furthermore, the expectation of the one-lag sample, $\hat{x}_1(x_0) \triangleq \mathbb{E}_{\kappa_1(x_1|x_0)}x_1$, for this distribution are given by

$$\hat{x}_h(x_0) = \theta + \frac{x_0 - \theta}{(a+1)^h}.$$

Intuitively, this characterizes how fast the expectation of the h -lag sample approaches the true distribution mean θ .

The relative difference $\frac{\hat{x}_h(x_0) - \theta}{x_0 - \theta}$ decays exponentially in h , with a factor of $\frac{1}{a+1}$. In fact, the $\rho(1)$ for the exponential family class of model introduced in Roberts & Tweedie (1996), with potential energy $E(x) = x^\omega, x \geq 0, \omega > 0$, can be analytically calculated. The result, provided in the Appendix, indicates that $\rho(1)$ decays at a rate of $\mathcal{O}(1/(a+1))$.

6.5 MG-HMC mixing performance

So far we have discussed the mixing properties of analytic MG-SS. In theory, the MG-HMC is expected to have the same theoretical property as the MG-SS. However, the mixing performance of the two methods could differ significantly, especially when sampling from a multimodal distribution.

To be more precise, as shown in Figure 2, suppose we are sampling from a bimodal distribution. There must exist a critical value y_T , such that when the slicing variable y exceeds y_T , the slice interval \mathbb{X} will have two disjoint components. Since the mapping between y and the Hamiltonian H is bijective, the corresponding Hamiltonian, H , will also have a critical value H_T , below which there would be two closed Hamiltonian contours associated with the same energy. The nature of Hamiltonian dynamics only allows moving along a single contour, whereas the analytic MG-SS is able to sample from distributions with disjoint domain, *i.e.*, \mathbb{X} having several disjoint components. As a consequence, the MG-HMC is expected to be less efficient than its analytic MG-SS counterpart. In order to move across different modes, the sampler has to have a large Hamiltonian, $H \geq H_T$.

To characterize the performance gap between the analytic MG-SS and MG-HMC, we note that from (11), the marginal distribution of H can be obtained as $p(H; a) = [H - E(x)]^{a-1} e^{-H} / [\Gamma(a) Z_1]$. Therefore,

$$\begin{aligned} P(H \geq H_T) &= \\ &= \int_{H \geq H_T} \frac{\int_{E(x) \leq H} [H - E(x)]^{a-1} dx}{\Gamma(a) Z_1} \times e^{-H} dH \\ &= 1 - \frac{1}{Z_1} \int_{E(x) \leq H_T} \frac{\gamma(a, H_T - E(x))}{\Gamma(a)} \times e^{-E(x)} dx, \end{aligned}$$

where $\gamma(\cdot, \cdot)$ denotes the lower incomplete Gamma function. Note that $P(a, x) = \frac{\gamma(a, x)}{\Gamma(a)}$ is the cumulative distribution function of Gamma($a, 1$), thus is monotonically decreasing with a , and as $a \rightarrow \infty, P(a, x) \rightarrow 0$. This implies that when a is large enough, the chances of reaching an energy level that restricts the traversing across modes can be arbitrarily small. As a result, in theory the MG-HMC with large value of a is particularly advantageous for sampling multimodal distributions.

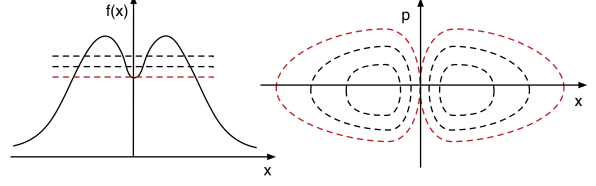


Figure 2: Left (sample space): critical value (red) of slicing variable y , above which the slice interval will be disjoint. Right (phase space): critical value (red) of the Hamiltonian H , above which the contour will have two disjoint components.

7 No free lunch

In order to obtain better mixing, the last section suggests choosing a as large as possible. However, this is not the case in practice because larger a will also lead to a less accurate numerical integrator. To see how this happens, consider sampling from a Laplace distribution, with potential energy defined as $E(x) = |x|$ and Hamiltonian $H(x, p) = |x| + |p|^{1/a}$. As a gets larger, the contour of the total Hamiltonian becomes more “stiff”, meaning that the maximum curvature becomes larger; see Figure 3. In fact, from (13), as $a \rightarrow \infty, \nabla K(\mathbf{p}) \rightarrow 0$. This requires either a larger step-size ϵ or a very small value of m to help the sampler make adequate moves. However, both of these two strategies introduce large numerical error.

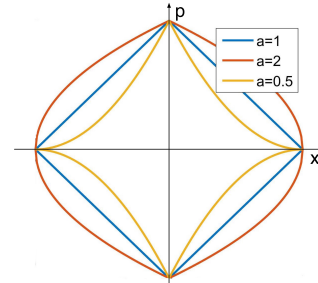


Figure 3: Hamiltonian contours for different a in phase space.

As a result, compromising between the theoretical advantage and numerical difficulty suggests an optimal a for distinct tasks. Empirically, we suggest to set a less than 3 when the dimension is large, because the numerical error usually grows faster than the theoretical mixing performance gain. Extensions that account for geometric information (Girolami & Calderhead, 2011) or using more accurate numerical integrator (Chao et al., 2015) may allow adopting larger values of a .

8 Experiments

8.1 Simulation studies

To validate the theoretical results, we performed empirical experiments on several simulated problems.

1D unimodal problems We evaluate the performance of the MG sampler with several univariate distributions $p(x) = \frac{1}{Z_1} \exp(-E(x))$, *s.t.* $x \geq 0$:

- 1) **Exponential distribution** $\text{Exp}(\theta)$, where $E(x) = \theta x$.
- 2) **Positive-truncated Gaussian** $\mathcal{N}_+(0, \theta)$, $E(x) = x^2$.
- 3) **Gamma distributions** $\text{Gamma}(r, \theta)$, where $E(x) = -(r-1) \log x + \theta x$, where $r = 2$ and $r = 3$

Note that the performance of the sampler does not depend on θ . We performed analytic MG-SS[§] and MG-HMC with leap-frog integration. Theoretically, the exponential distribution (case 1) and the positive-truncated Gaussian distribution (case 2) have closed-form autocorrelation and ESS. For positive-truncated Gaussian this is

$$\rho(1) = \frac{1}{(\pi/2 - 1)} \left[\frac{\Gamma(a + \frac{1}{2}) \Gamma(a + \frac{3}{2})}{\Gamma(a + 1)^2} - 1 \right].$$

In the Gamma distribution case (case 3), analytical derivation of the autocorrelations and ESS are difficult, thus we resort to a numerical approach to compute the theoretical results from (15). The details of computing the theoretical $\rho(1)$ and ESS in these cases can be found in the Appendix.

Each method was run for 30000 Monte Carlo iterations with 10000 burn-in samples. The leap-frog steps are set as 100 for each experiment (in practice, the leap-frog steps are uniformly drawn from $[100 - l, 100 + l]$, $0 < l < 100$, which has better convergence guarantee as suggested by Livingstone et al. (2016). The mass parameter m and step-size ϵ are selected according to the acceptance ratio (see details in the Appendix). In principle, as a becomes larger, it would be desirable to choose a smaller ϵ to compensate for the numerical hardness. The acceptance ratio decreases from around 0.98 to around 0.77 for each case, when a grows from 0.5 to 4. As shown in Figure 4, empirical results are consistent with theoretical autocorrelation and ESS. For the exponential and positive-truncated Gaussian cases, as a becomes larger, the autocorrelation decreases from 1 to a small value close to zero, meanwhile the ESS increases to approach the total sample size.

The analytic MG-SS almost exactly matches the theoretical results, however MG-HMC suffers more from numerical difficulties when a is large, thus it gradually deviates from the theoretical values. These numerical difficulties are exaggerated in the Gamma case (Figure 5), where

[§]Analytical MG-SS is only available for the exponential distribution and for the positive-truncated Gaussian when $a = \{0.5, 1, 2\}$. Details are provided in the Appendix.

the autocorrelation first decreases then becomes larger. Meanwhile, the acceptance ratio decreases from 0.9 to 0.5. Note that one may consider using a larger number of leap-frog updates with a smaller stepsize to make adequate moves while maintain a high acceptance ratio. However, this practice inevitably results in longer running time.

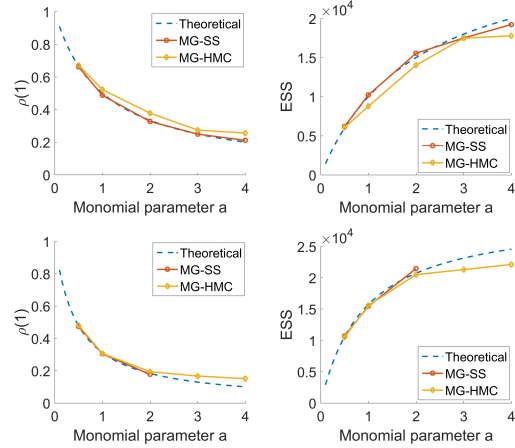


Figure 4: Theoretical and empirical $\rho(1)$ and ESS of exponential distribution (upper) and \mathcal{N}_+ (lower).

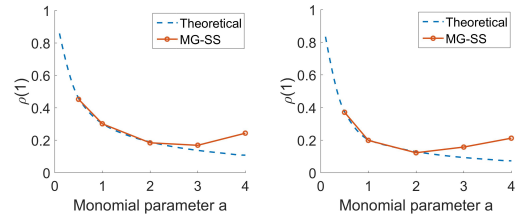


Figure 5: Theoretical and empirical $\rho(1)$ for Gamma distribution with parameters $r = 2$ (left) and $r = 3$ (right).

1D	ESS	$\rho(1)$	2D	ESS	$\rho(1)$
$a = 0.5$	5175	0.60	$a = 0.5$	4691	0.67
$a = 1$	10157	0.43	$a = 1$	16349	0.60
$a = 2$	24298	0.11	$a = 2$	18007	0.53

Table 1: Effective sample size of MG-HMC for 1D and 2D bimodal distributions.

1D and 2D bimodal problems We further conducted a simulated study to evaluate the efficiency of MG-HMC when sampling both 1D and 2D multimodal distributions. For the univariate case, we attempt to sample from a density where the potential energy is given by $E(x) = x^4 - 2x^2$. For the bivariate case, the potential energy function is given by $E(\mathbf{x}) = -0.2 \times (x_1 + x_2)^2 + 0.01 \times (x_1 + x_2)^4 - 0.4 \times (x_1 - x_2)^2$. The symmetry of the energy function implies

Dataset (dim)	Australian (15)	German (25)	Heart (14)	Pima (8)	Ripley (7)	Cavaran (87)
MG-HMC $a = 0.5$	3124	3447	3524	3434	3317	33 (median 3987)
MG-HMC $a = 1$	4308	4353	4591	4664	4226	36 (median 4531)
MG-HMC $a = 2$	1255	2853	2127	3109	1012	7 (median 607)

Table 2: Minimum effective sample size for each method (dimensionality of each dataset is indicated in parenthesis)

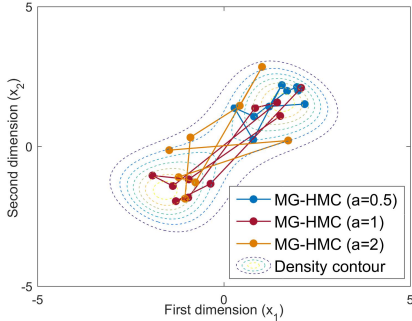


Figure 6: Sample results by MG-HMC from 2-D distribution. Only 10 samples are shown for clarity.

that, in theory, the analytic MG-SS will have ESS equal to the total sample size. However, the MG-HMC will have a performance gap *w.r.t.* analytic MG-SS. We run MG-HMC for $a = \{0.5, 1, 2\}$ for 30000 iterations with 10000 burn-in samples. Each leap-frog update has 50 steps with stepsize $\epsilon = 0.05$. Parameter settings and the acceptance ratio are detailed in the Appendix. Empirically, we found that the efficiency of HMC is significantly improved with a large value of a (Table 1). As shown in Figure 6, we observe that, empirically, the MG-HMC sampler with monomial parameter $a = \{1, 2\}$ performs better at jumping between modes of the target distribution than standard HMC.

100 dimensional multivariate Gaussian We also assessed the performance of MG-HMC for sampling a 100-dimensional Gaussian, where $a = 1$ outperforms $a = \{0.5, 2\}$. Settings and results are provided in the Appendix.

8.2 Real data

Bayesian logistic regression We evaluated our methods on 6 real-world logistic regression datasets from the UCI repository (Bache & Lichman, 2013): German credit, Australian credit, Pima Indian, Heart, Ripley and Caravan (Van Der Putten & van Someren, 2000). Feature dimensions range from 7 to 87 and total data instances are between 250 to 5822. All datasets are normalized to have zero mean and unit variance. The mass matrix $\mathbf{M} = m\mathbf{I}$, where m is mass parameter. Gaussian priors $\mathcal{N}(\mathbf{0}, 100\mathbf{I})$ were imposed on the regression coefficients.

For each dataset we drew 5000 MC samples with 1000

burn-in samples. The leap-frog steps were set to be uniformly drawn from 1 to 100, as suggested by Neal (2011). We manually select the stepsize and mass parameter m , so that the acceptance ratios fall in $[0.6, 0.9]$ (Betancourt et al., 2014) (see Appendix for parameter settings). On each dataset, the running time for each method is roughly identical, due to the fact that each method takes approximately the same number of leap-frog steps.

Results are summarized in Table 2. We evaluate each method in terms of minimum ESS. MG-HMC with $a = 1$ outperforms the other two settings, $a = 0.5$ and $a = 2$. Despite the performance gain from using MG-HMC with a large a , numerical difficulties arise dramatically in this scenario, which pushes the optimal value of a towards zero. This can be validated by the acceptance ratio drop from around 0.9 to around 0.7 as a increases from 0.5 to 2 for each dataset. We also observed that the dimensionality seems to have an impact on the optimal setting of a . For high-dimensional problems such as Cavaran, though MG-HMC with $a = 1$ still outperforms standard HMC where $a = 0.5$, the improvement is less significant than with other datasets. Though the increasing numerical difficulty is inevitable, one can still reduce the numerical error by employing sophisticated numerical methods to move the optimum a to a large value, thereby keeping the advantage over standard HMC. Since all MG samplers can be shown invariant to true posterior, we did not compare the accuracy.

ICA We also evaluate our methods on the MEG (Vigário et al., 1998) dataset for Independent Component Analysis (ICA), containing 17730 time points. We used the first 5 channels, resulting in 25 feature dimensions. All experiments are based on 5000 MCMC samples. The settings for the model and parameter are provided in the Appendix. As shown in Table 3, when $a = 1$, MG-HMC has better mixing performance compared with other settings.

	min ESS	Time(s)	AR
$a = 0.5$	2677	525	0.98
$a = 1$	3029	517	0.97
$a = 2$	1534	512	0.77

Table 3: Results for ICA on MEG data. $d = 5, N = 17730$.

References

- Bache, Kevin and Lichman, Moshe. UCI machine learning repository, 2013.
- Betancourt, Michael, Byrne, Simon, and Girolami, Mark. Optimizing the integrator step size for Hamiltonian Monte Carlo. *arXiv preprint arXiv:1411.6669*, 2014.
- Brooks, Steve, Gelman, Andrew, Jones, Galin, and Meng, Xiao-Li. *Handbook of Markov Chain Monte Carlo*. CRC press, 2011.
- Chao, Wei-Lun, Solomon, Justin, Michels, Dominik, and Sha, Fei. Exponential integration for Hamiltonian Monte Carlo. In *ICML*, 2015.
- Duane, Simon, Kennedy, Anthony D, Pendleton, Brian J, and Roweth, Duncan. Hybrid Monte Carlo. *Physics letters B*, 195(2):216–222, 1987.
- Fu, Wenjiang J. Penalized regressions: the bridge versus the lasso. *Journal of computational and graphical statistics*, 7(3):397–416, 1998.
- Girolami, Mark and Calderhead, Ben. Riemann manifold Langevin and Hamiltonian Monte Carlo methods. *Journal of the Royal Statistical Society: Series B (Statistical Methodology)*, 73(2):123–214, 2011.
- Goldstein, Herbert. *Classical mechanics*. Pearson Education India, 1965.
- Homan, Matthew D and Gelman, Andrew. The no-u-turn sampler: Adaptively setting path lengths in hamiltonian monte carlo. *The Journal of Machine Learning Research*, 15(1):1593–1623, 2014.
- Isaac, Richard. A general version of doebelin’s condition. *The Annals of Mathematical Statistics*, pp. 668–671, 1963.
- Jiang, Chengxiang and Cong, Yuhao. A sixth order diagonally implicit symmetric and symplectic Runge-Kutta method for solving hamiltonian systems. *Journal of Applied Analysis and Computation*, 5(1):159–167, 2015.
- Johnson, Alicia A. *Geometric ergodicity of Gibbs samplers*. PhD thesis, university of Minnesota, 2009.
- Livingstone, Samuel, Betancourt, Michael, Byrne, Simon, and Girolami, Mark. On the Geometric Ergodicity of Hamiltonian Monte Carlo. *ArXiv*, January 2016.
- Murray, Iain, Adams, Ryan Prescott, and MacKay, David JC. Elliptical slice sampling. *ArXiv*, 2009.
- Nadarajah, Saralees. A generalized normal distribution. *Journal of Applied Statistics*, 32(7):685–694, 2005.
- Neal, Radford M. Slice sampling. *Annals of statistics*, pp. 705–741, 2003.
- Neal, Radford M. MCMC using Hamiltonian dynamics. *Handbook of Markov Chain Monte Carlo*, 2, 2011.
- Pakman, Ari and Paninski, Liam. Auxiliary-variable exact Hamiltonian Monte Carlo samplers for binary distributions. In *NIPS*, 2013.
- Robert, Christian and Casella, George. *Monte Carlo statistical methods*. Springer Science & Business Media, 2004.
- Roberts, Gareth O and Rosenthal, Jeffrey S. Markov-chain Monte Carlo: Some practical implications of theoretical results. *Canadian Journal of Statistics*, 26(1):5–20, 1998.
- Roberts, Gareth O and Tweedie, Richard L. Exponential convergence of Langevin distributions and their discrete approximations. *Bernoulli*, pp. 341–363, 1996.
- Rosenthal, Jeffrey S. Minorization conditions and convergence rates for Markov chain Monte Carlo. *Journal of the American Statistical Association*, 90(430):558–566, 1995.
- Salimans, Tim, Kingma, Diederik P, and Welling, Max. Markov chain Monte Carlo and variational inference: Bridging the gap. *ArXiv*, 2014.
- Striebel, Michael, Günther, Michael, Knechtli, Francesco, and Wandelt, Michèle. Accuracy of symmetric partitioned Runge-Kutta methods for differential equations on Lie-groups. *ArXiv*, 12 2011.
- Taylor, John Robert. *Classical mechanics*. University Science Books, 2005.
- Tierney, Luke and Mira, Antonietta. Some adaptive Monte Carlo methods for Bayesian inference. *Statistics in Medicine*, 18(1718):2507–2515, 1999.
- Van Der Putten, Peter and van Someren, Maarten. COIL challenge 2000: The insurance company case. *Sentient Machine Research*, 9:1–43, 2000.
- Vigário, Ricardo, Jousmäki, Veikko, Hämmäläinen, M, Haft, R, and Oja, Erkki. Independent component analysis for identification of artifacts in magnetoencephalographic recordings. In *NIPS*, 1998.
- Zhang, Yichuan, Ghahramani, Zoubin, Storkey, Amos J, and Sutton, Charles A. Continuous relaxations for discrete Hamiltonian Monte Carlo. In *NIPS*, 2012.